S.T. Yau High School Science Award

Research Report

The Team

Name of team member: Ellen Wang
School: Horace Mann School
City, Country: Bronx, NY, USA

Name of supervising teacher: Joan Wang
Job Title: Professor
School/Institution: Department of Physics, Xiamen University Malaysia
City, Country: Sepang, Malaysia

Title of Research Report

A Study on Arctic Sea Ice Dynamics Using the Continuous Spin Ising Model

Date

August 20th, 2023

A Study on Arctic Sea Ice Dynamics Using the Continuous Spin Ising Model

Ellen Wang[1*]

[1] Horace Mann School, Bronx, NY, USA

*** Correspondence:**

Ellen_Wang@horacemann.org

Abstract

The Ising model, initially proposed about 100 years ago to explain ferromagnetism, has become a central pillar of statistical physics and a powerful tool for numerous applications in other fields including environmental studies. In this paper, we introduce continuous spin values to a two-dimensional Ising model and utilize the generalized Ising lattice to simulate the dynamics of sea ice/water transition in the Arctic region. The simulation process follows the Metropolis-Hastings algorithm and incorporates an innovative factor to account for the inertia of spin value changes. Using the sea ice concentration data collected by the National Snow and Ice Data Center, our model simulation shows striking similarity with the observed ice melting and freezing dynamics. Two numerical measures from the simulation, the average ice coverage and the ice extent, match closely with the observations. Moreover, the model's best-fit parameters demonstrate substantial impact of external forces, which can be further enriched and linked to the environmental factors in other climate change models. Based on our model and our simulation results, the Arctic sea ice extent in September 2023 is predicted to be the second lowest in history, near the minimum achieved in 2012.

Keywords: *Ising model, continuous spin, Metropolis-Hastings algorithm, phase transition, Arctic sea ice, climate change*

Acknowledgements

We thank the National Snow and Ice Data Center (NSIDC) and the National Aeronautics and Space Administration (NASA) for generously making the data publicly available and providing data support for this research.

We thank Professor Joan Wang for her encouragement and valuable comments. We also thank the Science Research course offered by Horace Mann School for the introduction of various research methodologies and the access to extensive physics literature. Moreover, we are grateful to the Summer Research Program at the Western Connecticut State University Department of Mathematics for the learning opportunities of advanced simulation, optimization, and machine learning methods.

Commitments on Academic Honesty and Integrity

We hereby declare that we

1. are fully committed to the principle of honesty, integrity and fair play throughout the competition.
2. actually perform the research work ourselves and thus truly understand the content of the work.
3. observe the common standard of academic integrity adopted by most journals and degree theses.
4. have declared all the assistance and contribution we have received from any personnel, agency, institution, etc. for the research work.
5. undertake to avoid getting in touch with assessment panel members in a way that may lead to direct or indirect conflict of interest.
6. undertake to avoid any interaction with assessment panel members that would undermine the neutrality of the panel member and fairness of the assessment process.
7. observe the safety regulations of the laboratory(ies) where we conduct the experiment(s), if applicable.
8. observe all rules and regulations of the competition.
9. agree that the decision of YHSA is final in all matters related to the competition.

We understand and agree that failure to honour the above commitments may lead to disqualification from the competition and/or removal of reward, if applicable; that any unethical deeds, if found, will be disclosed to the school principal of team member(s) and relevant parties if deemed necessary; and that the decision of YHSA is final and no appeal will be accepted.

(Signatures of full team below)

X ______________________________

Name of team member: Ellen Wang

X Joan Wang ______________________________

Name of supervising teacher: Joan Wang

Table of Contents

List of Figures

List of Tables

1 Introduction

1.1 Ising model

The Ising model (IM) was first formalized by physicists Ernst Ising and Wilhelm Lenz to explain the equilibrium and the phase transition in magnetic systems. The one-dimensional (1-D) IM was solved by Ising in his 1924 thesis [1] [2] [3], which proves the non-existence of phase transition in the 1-D IM. In 1944, Lars Onsager [4] was able to solve the two-dimensional (2-D) square-lattice IM analytically. Contradictory to the 1-D case, Onsager identified that there exists a critical temperature $T_c = 2.27\ J/k_B$ when the phase transition happens in a 2-D IM. Later studies of IM in higher dimensions have been closely associated with various developments in advanced 20th-century physics and mathematical theories, including the transfer-matrix method, quantum field theory, mean-field theory, etc.

Over the years, the IM has found wide success beyond physics. Specifically, the Kinetic IM [5] [6] [7], built upon the equilibrium version, has been proposed to analyze biology, environmental science, machine learning [8] [9], social science, and economic and financial systems. These applications are usually implemented as a discrete time Markov chain of the spin lattice, with spin interactions bounded to finite distance. In biology and neuroscience, the IM applications include but are not limited to the condensation of DNA [10], genetics [11], neural networks [12] [13], neuron spike [14], neuron activity in cell assemblies [15], and ligands to receptors binding in cells [16]. In environmental science, it has been employed to investigate land pattern dynamics [17] [18] and the equilibrium configuration of ice melt ponds [19]. In social science, economics, and finance, the IM has been applied to research in urban segregation [20], crisis study [21], stability of money [22], etc.

1.2 Arctic sea ice

The reversible phase transition between water and ice makes the IM a great tool to study the dynamics of a surface region with the co-existence of both states. In this paper, we apply a 2-D IM lattice to study the dynamics of Arctic sea ice melting and freezing cycles, a major climate change indicator that is of great environmental, economic and social significance.

Sea ice is undoubtedly an integral part of the Arctic Ocean and the earth [23]. In the dark winter months, ice almost covers entirety of the Arctic Ocean, and the ice extent—defined as the percentage of areas that are covered by at least 15% of ice—and the ice thickness typically reach their peaks around March. Starting in late spring, ice melting gradually exceeds water freezing due to higher temperatures and longer hours of sunlight exposure. Sea ice typically reaches the minimum extent and thickness in mid-September, when ice coverage can drop to under half of the winter maximum [24]. After mid-September, sea water freezing starts to exceed ice melting, so ice coverage expands. This cycle repeats annually.

Ice coverage is widely acknowledged as a crucial indicator of global climate change. Albedo, the percentage of incident light reflected from the surface of the earth, is highly dependent on the ice extent [25]. Light-colored ice or snow reflects more light than blue-colored liquid water; therefore, they are essential to keeping the Arctic at a cooler temperature and subsequently maintaining the energy balance around the globe. If the energy balance is broken, as ice decline has been detected in recent years, the feedback loop effect may occur, i.e., less reflection and more absorption of solar energy lead to even more ice loss and further global warming. Moreover, the Arctic ecosystem is directly impacted by the change in the sea ice coverage, which, for instance, threatens the lives of polar bears and walruses who rely on sea ice for hunting and breeding. Nevertheless, the diminishing of Arctic sea ice may present social and economic opportunities. For example, the once freezingly cold Arctic regions, such as Greenland, may be more habitable to humans.

Data recorded by the National Aeronautics and Space Administration (NASA) and the National Snow and Ice Data Center (NSIDC) since 1979 has shown declines in both ice extent and thickness in the Arctic, with year-over-year fluctuations in either direction. The lowest Arctic sea ice extent was observed in September of 2012 [26] [27]; between 2013 and 2022, the ice extent has been higher than the 2012 minimum, but still much lower than the average of the past four decades. This past month, July 2023, has just been reported as the hottest month of the earth on record [28]. A natural question then comes to us: will the Artic sea ice extent break the 2012 minimum? As we await the answer for another month, our paper makes a prediction based on the IM simulation projection in a focus Arctic region.

2 Theoretical framework

2.1 Classical Ising model

The system described by an IM is a set of lattice sites, each having a spin that interacts with its neighbors. The Hamiltonian function [1] [2] [3] for the lattice σ in a standard IM is given as

$$H(\sigma) = -\sum_{<i,j>} J_{ij}\sigma_i\sigma_j - \sum_i B_i\sigma_i, \tag{1}$$

where σ_i represents the spin variables at site i, taking the values of +1 or -1, J_{ij} represents the interaction between sites, and B_i represents the interaction of the external field with the spin at site i. i and j range across the full lattice, which can be one, two or higher dimensions, and $<i,j>$ represents pairs of spins that interact with each other. In the usual scenario, each spin only interacts with its nearest neighbors, so $<i,j>$ sums over all adjacent sites. For example, in a simple 2-D IM, each spin interacts only with four sites that are directly left, right, above and under. J_{ij} is usually positive, meaning that adjacent spins are inclined to maintain the same value to achieve low energy.

In statistical physics, the configuration probability follows the Boltzmann distribution [29]

$$P_\beta = \frac{e^{-\beta H(\sigma)}}{Z_\beta}, \tag{2}$$

where Z_β is the partition function:

$$Z_\beta = \sum_\sigma e^{-\beta H(\sigma)}, \tag{3}$$

and

$$\beta = (k_B T)^{-1}. \tag{4}$$

β is the inverse temperature; k_B is the Boltzmann constant; T is the IM temperature (it is called IM temperature in this paper to differentiate from the ambient temperature that will also be discussed for our sea ice freezing and melting studies).

The evolution of the kinetic IM runs through a series of spin flips over the lattice. The probability of each spin flip depends on whether such flip increases or reduces energy. Mathematically the probability is determined by $e^{-\beta(H_v - H_\mu)}$, where H_v and H_μ represents the Hamiltonian of the system before and after the flip. It can be easily seen that higher IM temperature leads to more thermal fluctuations and greater randomness in the spin value distribution, while lower IM temperature shows less fluctuations.

2.2 Continuous Spin Ising model

Most studies of the IM focus on binary values of the spins, i.e., σ_i taking values of +1 or -1 only. However, the sea ice data for each lattice location takes varying values between 0 and 1 that represents the percentage of ice coverage. Therefore, we generalize the IM to allow for continuous spin values that can take any real number between -1 and +1. This generalization enables the IM to examine more realistic systems, but also adds a high degree of complexity to the mathematical solutions. Past research has studied phase transitions and critical behavior of continuous IM [30] [31]. Recently, an IM with variable power-law spin strengths was studied with its rich phase diagram [32].

The Hamiltonian function of continuous spin IM is represented by the same Equation (1). However, σ_i now takes continuous values between $+1$ and -1;$-J_{ij}\sigma_i\sigma_j$ reaches the minimum energy state if $\sigma_i = \sigma_j = +1$, or $\sigma_i = \sigma_j = -1$, as the energy of any other values of the pairs will be higher. The highest energy is observed when $\sigma_i = +1, \sigma_j = -1$, or vice versa. This numeric feature works ideally for ice/water lattice: the most stable low energy state is either 100% water or ice, whereas ice next to water is the most unstable high energy state.

2.3 Monte Carlo simulation and inertia factor

The incorporation of the continuous spins also adds to the complexity of the Monte Carlo (MC) simulation of the IM lattice. In the classical binary spin IM, σ_i can only flip to -σ_i in each simulation step, and therefore the absolute value of the change is always 2 no matter the flip goes from -1 to +1, or from +1 to -1. In a continuous IM, the challenge to determine the post-flip numeric value of the new spin arises. In our approach, this new spin is implemented through a random number. However, what is the random distribution that the new spin value should follow? How does the spin value change, i.e. $\Delta\sigma_i$, affect the dynamics of the IM? To address these questions, we introduce an innovative inertia factor I, and the probability of each flip will be determined by

$$P_{flip} = e^{-\beta(H_\nu - H_\mu + I|\sigma'_i - \sigma_i|)}, \tag{5}$$

where H_ν and H_μ still represent the system Hamiltonian before and after the flip. The newly added $-I|\sigma'_i - \sigma_i|$ accounts for the energy needed to overcome the inertia of the spin change, and I is an IM parameter to be fitted. Intuitively speaking, this term represents the natural resistance to state change, or can be thought of as the latent heat needed for the water/ice phase transition in classical thermodynamics.

Here is an example to illustrate the inertia effect. Starting with an initial spin value of 0.8, a flip to either 0.7 or 0.6 may result in the same system Hamiltonian value for the new lattice. However, we differentiate these two new states by assigning higher probability for the flip to 0.7 because the spin change is smaller. In Equation (5), $-I|\sigma'_i - \sigma_i|$ determines the distribution of new spin values, and in practice, it significantly improves the simulation results to match the observations.

In summary, we have introduced two new features to the classical IM: the continuous spin values and an inertia factor. These mathematical additions prepare us to study the real-world Arctic sea ice dynamics.

3 Data description

Our study uses the data of "Near-Real-Time DMSP SSMIS Daily Polar Gridded Sea Ice Concentrations" (NRTSI) [33] from the National Snow and Ice Data Center (NSIDC), which collects daily sea ice concentrations for both the Northen and Southern Hemispheres. The Special Sensor Microwave Imager/Sounder (SSMIS) on the NANA Defense Meteorological Satellite Program (DMSP) satellites acquires the near-real-time passive microwave brightness temperatures, which serve as inputs to NRTSI dataset using the NASA Team algorithm to generate the sea ice concentrations.

The NRTSI files are in netCDF format. Each file of the Arctic region contains a lattice of 448 rows by 304 columns, covering a large earth surface area with the north pole at the center. Each grid cell represents an area of approximately 25 kilometers by 25 kilometers. The value for each grid cell is an integer from 0 to 250 that indicates the fractional ice coverage scaled by 250. 0 indicates 0% of ice concentration; 250 indicates 100% of ice concentration. The image of part of the NRTSI file on Sept 16th, 2022 is illustrated in Figure 1 (a). In the map, white represents ice, blue represents water and gray is land. The exact north pole location is covered by a gray circular mask because of the limitation of the satellite sensor measurement caused by the orbit inclination and instrument swath.

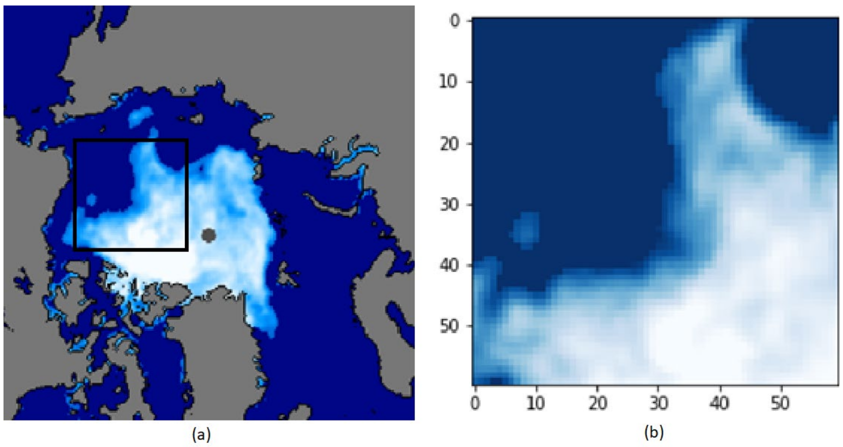

Figure 1: (a) Part of the NRTSI data on Sept 16th, 2022; (b) The focus area for our research, which is a 60x60 square lattice covering approximately 2.25 million square kilometers.

For this research paper, we focus on studying a specific geographic region bounded by the black square in Figure 1 (a), ranging from the East Siberian Sea (to the top of the box) and the Beaufort Sea (to the left of the box) to near the polar point; a zoom-in image of this focus area is shown in Figure 1 (b) . This large square area is unobstructed by lands or the north pole mask, making it an ideal field for the IM lattice setup. The area contains 60 rows and 60 columns in the data file, covering approximately 1500km x 1500km, or about 2.25 million square kilometers.

4 Ising model lattice and simulation setup

4.1 Ising model lattice

We first transform NRTSI data of the focus region as shown in Figure 1 (b) to Ising style data. A simple linear mapping is applied to convert integers from 0 to 250 to real numbers from -1 to +1. -1 indicates the cell is 100% ice; +1 indicates 100% water; 0 indicates 50%/50% coverage of water/ice. Each cell covers 25km x 25km of the total 1500km x 1500km focus region, and therefore a 60x60 matrix is initialized as the 2-D IM lattice for our study.

4.2 Simulation periods

Figure 2 (a) and (b) show an example of the initial and the final target states of an IM lattice simulation run. The simulation periods are chosen to be consistently half a month apart, for example, Sept 16th, 2022 in Figure 2 (a) and Oct 1st, 2022 in Figure 2 (b). This semi-monthly frequency is chosen to balance two considerations. First, the period is sufficiently long to allow for meaningful differentiation of the ice/water configuration between the start and the end dates; second, the period is not excessively too long and allows the IM simulation to mimic the daily water/ice configuration evolution on the interim dates between the start and the end, which is to be illustrated in Section 5.2.

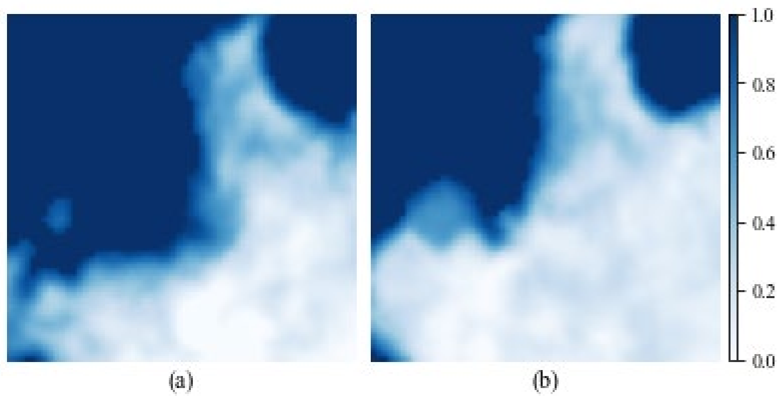

Figure 2: The initial and the final target states of an IM lattice simulation run. (a) shows our focus area on Sept 16th, 2022 and (b) Oct 1st, 2022. Each full simulation period is half a month.

4.3 Ising model parameters

In the IM Hamiltonian function, i.e., Equation (1), we set the following:

- σ_i is a real number between -1 and +1 for any cell i in our focus area.
- $<i,j>$ sums over all adjacent cells, so each spin interacts only with four sites that are directly left, right, above and under.
- J_{ij} is set to be constant within each simulation period across all cells.
- B_i is set to be time-invariant within each simulation period. However, in order to capture the real-world external force variation across locations, especially the environmental differences from the coast area to the north pole, B_i is set to be a linear function of x and y coordinates, i.e. $B_i = B_0 + B_x(x - x_0) + B_y(y - y_0)$, where B_0 is the average B over the lattice; x_0 and y_0 are the coordinates of the lattice center.
- I, the inertia factor, is set to be constant within each simulation period.
- β, the inverse Boltzmann temperature, is set to 1 without the loss of generality.

4.4 *Metropolis simulation steps*

Various MC methods have been developed for the IM simulation. Among them the most widely used are the Glauber dynamics [34] and the Metropolis-Hasting algorithm [35]. In our research, we follow the latter for the MC simulation of the IM lattice evolution. As described in Section 2.3, an inertia factor is introduced into our model and the generalized Metropolis-Hastings MC steps are as below:

1. Select cell i at random from the 2-D lattice of the focus area. Let spin value of this cell be σ_i.
2. Generate another random variable σ'_i between -1 and +1.
3. Compute the energy change ΔH_i from σ_i to σ'_i.
4. Compute the energy $I|\sigma'_i - \sigma_i|$ to overcome the inertia of changing spin value at i.
5. Compute the total energy change $\Delta E = \Delta H_i + I|\sigma'_i - \sigma_i|$.
6. (a) If ΔE is negative, the energy change is favorable since the energy is reduced. The spin value change is therefore accepted to σ'_i.
   (b) If ΔE is positive, the probability of spin flip is determined by the Boltzmann distribution. In this case, another random variable r between 0 and 1 is generated. If r is less than $P = e^{-\beta\Delta E}$, the spin value change is accepted; otherwise, the change is rejected and the spin value at i stays at σ_i.

For each semi-monthly simulation period, we repeat the above MC steps 50,000 times. As the lattice of our focus area has 3,600 cells, this repetition allows approximately 14 flip tries for each cell, or roughly once per day. This specific repetition number is an intuitive pick, which takes into account the computational complexity of the algorithm. Obviously, other choices of the repetition number can be considered as well. The fitted parameter values (J, B_0, B_x, B_y, I) might vary with different repetition numbers.

4.5 *Dual annealing optimization*

Our goal is to match the observed final state lattice configuration as closely as possible upon the completion of the IM simulations. In this research, the similarity between the observed and the simulated lattice configurations is measured by the sum of the absolute spin value differentials across the lattice. Mathematically, this is the Manhattan distance (as opposed to the more commonly used Euclide distance) between the observed and the simulated matrices.

Finally, we fit the values of parameters (J, B_0, B_x, B_y, I) to maximize of the similarity measure, i.e., to minimize the sum of the absolute spin value differentials. The minimization is done with the dual annealing optimization method, which combines fast local search with classical simulated annealing to achieve the global minimization solution [36] [37]. Description of the dual annealing method can be found in the Python SciPy package.

5 Results

We employ the continuous spin IM to simulate the dynamics of the sea ice/water transition for the focus Arctic Sea area. Thanks to the NRTSI data, we can conduct the simulation for every year in the past four decades.

5.1 Simulation results for 2022

We start with the most recent year 2022.

Figure 3 shows the semi-monthly NSIDC sea ice images of our focus area from June 16th, 2022 to Jan 1st, 2023. As can be seen, the melting cycle starts from June 16th and goes until Sept 16th, and the freezing cycle from Sept 16th to year end. Prior to June 16th, the region is almost fully covered by ice so the IM simulation will be trivial. Therefore, we set the simulation start date on June 16th of each year. During the period of June 16th to Dec 16th, every succeeding image shows considerable ice coverage difference from the previous date while retaining certain core features. This semi-monthly frequency choice allows our IM simulation to capture the essence of the evolution dynamics without overfitting the model.

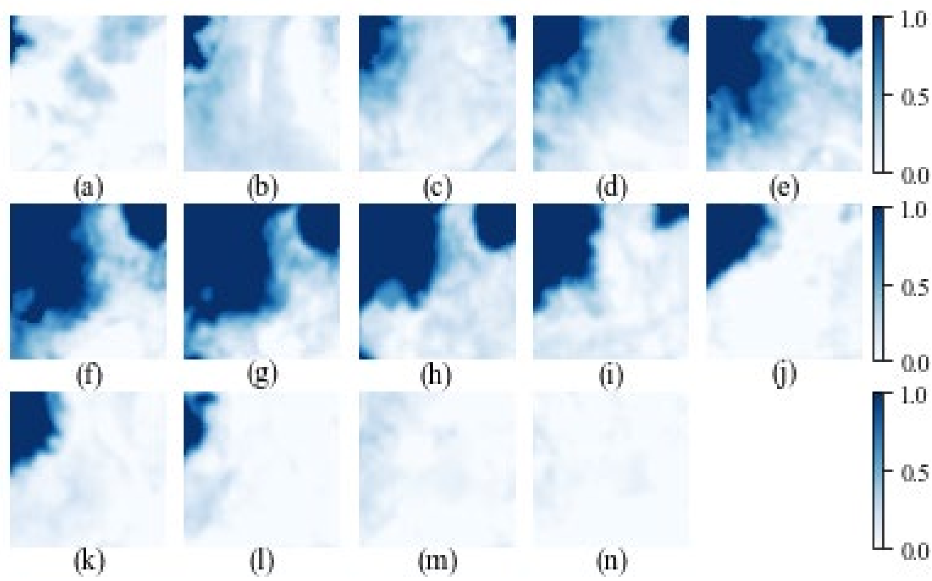

Figure 3: The actual semi-monthly evolution of sea ice in our focus area in 2022: (a) June 16th, 2022, (b) July 1st, (c) July 16th, (d) Aug 1st, (e) Aug 16th, (f) Sept 1st, (g) Sept 16th, (h) Oct 1st, (i) Oct 16th, (j) Nov 1st, (k) Nov 16th, (l) Dec 1st, (m) Dec 16th, (n) Jan 1st, 2023. Blue color indicates water; white indicates ice. The darker the color on each cell, the higher water concentration, as shown by the scale on the right.

The best-fit parameters for each simulation period based on dual-annealing minimization are shown in Table 1. The spin interaction coefficient J and the inertia factor I are relatively stable across periods. Whereas, the external force parameters B_0, B_x, and B_y display large variations across different time periods. In particular, the average force B_0 is positive from

June 1st to Sept 16th but turns negative afterwards, which can be explained intuitively by the seasonal ambient temperature as the dominant external factor for the ice/water dynamics. Ambient temperature is not the only factor though. Arctic temperature usually peaks in July/August while B_0 remains positive and ice melting continues through mid-September. This lagging effect could be explained by other environmental effects such as albedo or jet streams but is beyond the scope of this paper.

	6/16 to 7/1	**7/1 to 7/16**	**7/16 to 8/1**	**8/1 to 8/16**	**8/16 to 9/1**	**9/1 to 9/16**	**9/16 to 10/1**	**10/1 to 10/16**	**10/16 to 11/1**	**11/1 to 11/16**	**11/16 to 12/1**	**12/1 to 12/16**	**12/16 to 1/1/2023**
J	4.5	5.2	4.5	4.9	5.5	4.6	5.2	5.5	5.2	5.1	4.7	5.5	5.5
Bo	7.0	2.0	6.5	9.1	4.3	3.6	-12.6	-12.7	-14.9	-9.6	-15.0	-13.1	-14.4
Bx	0.2	-9.7	-5.5	3.7	-7.5	-8.2	-10.0	-6.1	-8.5	9.7	-1.9	-0.8	-3.1
By	-10.0	3.0	3.7	1.0	-6.4	2.9	0.1	-8.4	-5.6	-10.0	-5.9	5.4	-8.0
I	10.3	9.1	11.0	10.8	10.7	10.9	10.6	9.3	9.4	10.4	9.1	10.9	10.8

Table 1: Best-fit parameters of 2022 sea ice evolution.

The simulated sea ice images for each 2022 period are shown in Figure 4 utilizing the best-fit parameters in Table 1. These images exhibit excellent similarity to Figure 3, demonstrating the strong explanatory power of our Ising model. Nevertheless, our model is far from perfect. Upon close inspection, The images in Figure 3 and Figure 4 do reveal discrepancies, especially as shown in image (e) for Aug 16th, 2022, where the actual ice configuration displays significant irregularity compared to the prior period. While an IM with simple parameters encounters difficulties in describing these local irregularities, it is possible to include a richer set of parameters or to employ more complicated parametric functional forms of them at the potential cost of overfitting. In this paper, we keep our Ising model simple and accept these local discrepancies.

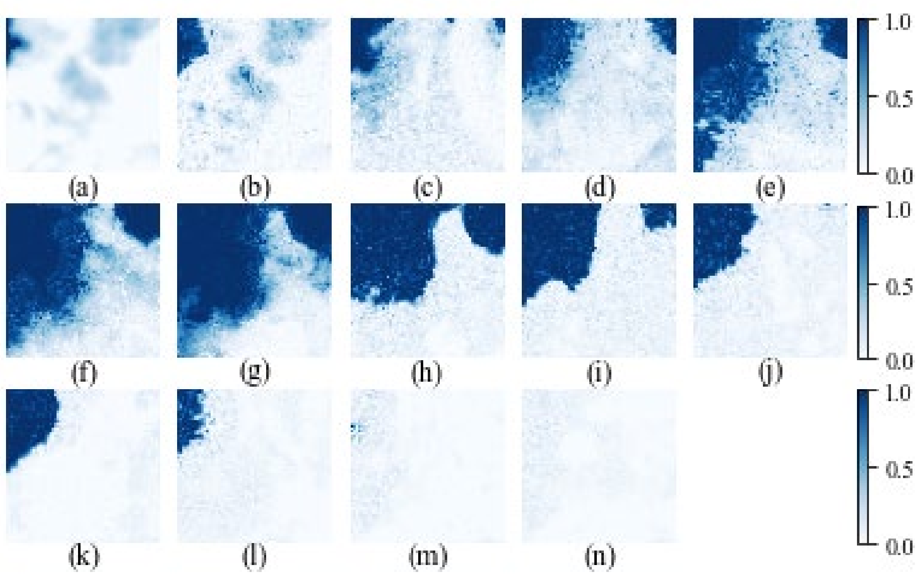

Figure 4: The simulated semi-monthly evolution of sea ice for our focus area in 2022. (a) is the actual image on June 16th, 2022 as the start state; (b)-(n) are simulated images on (b) July 1st, (c) July 16th, (d) Aug 1st, (e)

Aug 16th, (f) Sept 1st, (g) Sept 16th, (h) Oct 1st, (i) Oct 16th, (j) Nov 1st, (k) Nov 16th, (l) Dec 1st, (m) Dec 16th, and (n) Jan 1st, 2023.

To quantify the similarity between the IM simulations and the observations, we compute two key numerical measures for our focus area: the average ice coverage percentage, i.e., the mean of the ice coverage percentage over the lattice, and the ice extent, i.e., the percentage of areas that are covered by at least 15% of ice. The comparison results are shown in Figure 5. As anticipated, we see excellent match on both figures, although the results do show marginal but non-trivial discrepancy. It is interesting to notice that the simulated average ice coverage is usually higher than the actual measures, but the simulated ice extent is usually lower than the actual, a pattern that can be further investigated in future research.

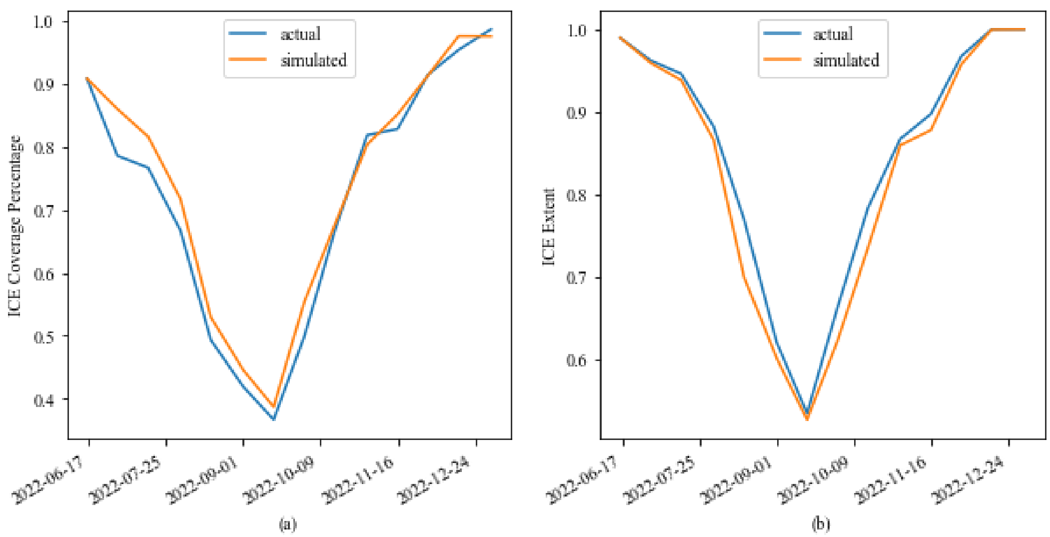

Figure 5: (a) The average ice coverage percentage in our focus area from June 16th, 2022 to Jan 1st, 2023; (b) The sea ice extent (the percentage of areas with at least 15% of ice coverage) from June 16th, 2022 to Jan 1st, 2023. Blue curves are the actual measures from the NRTSI data; orange ones show the IM simulation results.

5.2 *Daily sea ice evolution*

Do our semi-monthly IM simulation results match the actual sea ice dynamics on a smaller time scale? To answer this question, we utilize the semi-monthly best-fit parameters in Table 1 to simulate the daily evolution. Two periods, a melting period from Aug 16th to Sept 1st, 2022, and a freezing period from Oct 16th to Nov 1st, 2022, are simulated day-by-day for this exercise. The results, with comparisons between the actual and the simulated daily ice evolution, are shown in Figure 6 to Figure 9. The comparisons exhibit striking similarity over all the daily images in both periods, demonstrating that our IM model preserves the more granular ice/water dynamics.

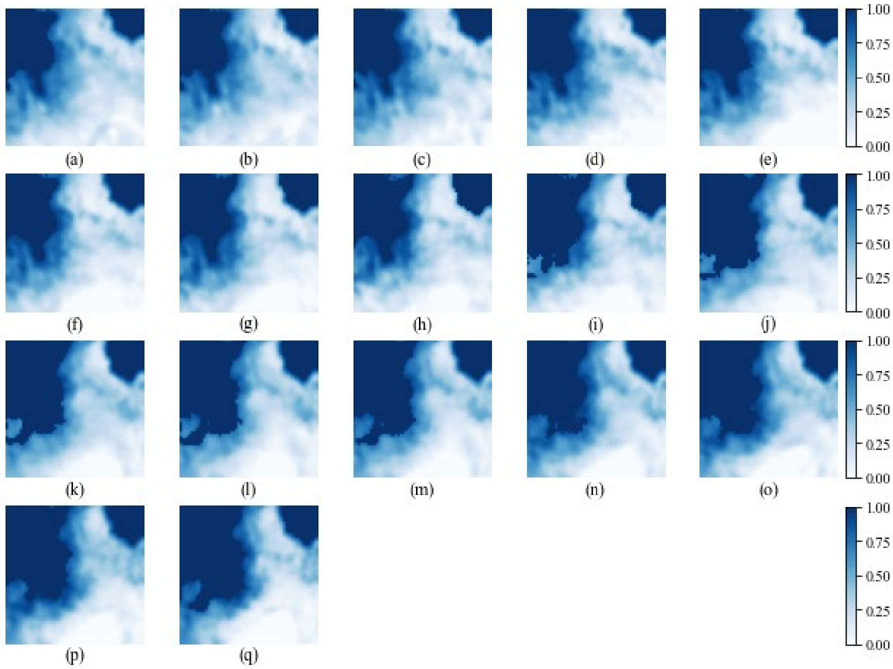

Figure 6: The actual daily evolution of sea ice in our focus area during a melting cycle from (a) Aug 16th, 2022 to (q) Sept 1st, 2022.

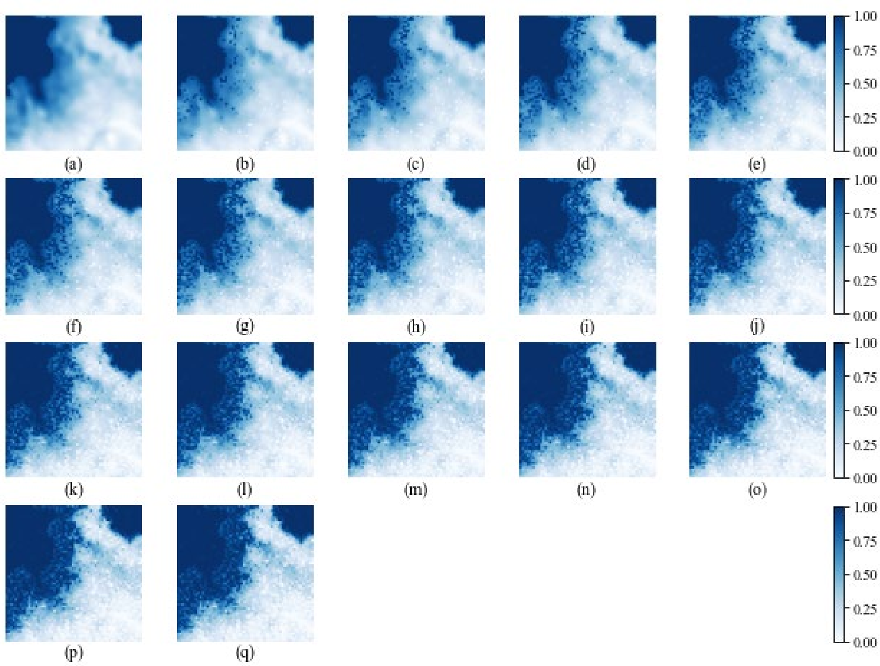

Figure 7: The simulated daily evolution of sea ice, based on the semi-monthly best-fit parameters, for our focus area during a melting cycle from (a) Aug 16th, 2022 to (q) Sept 1st, 2022.

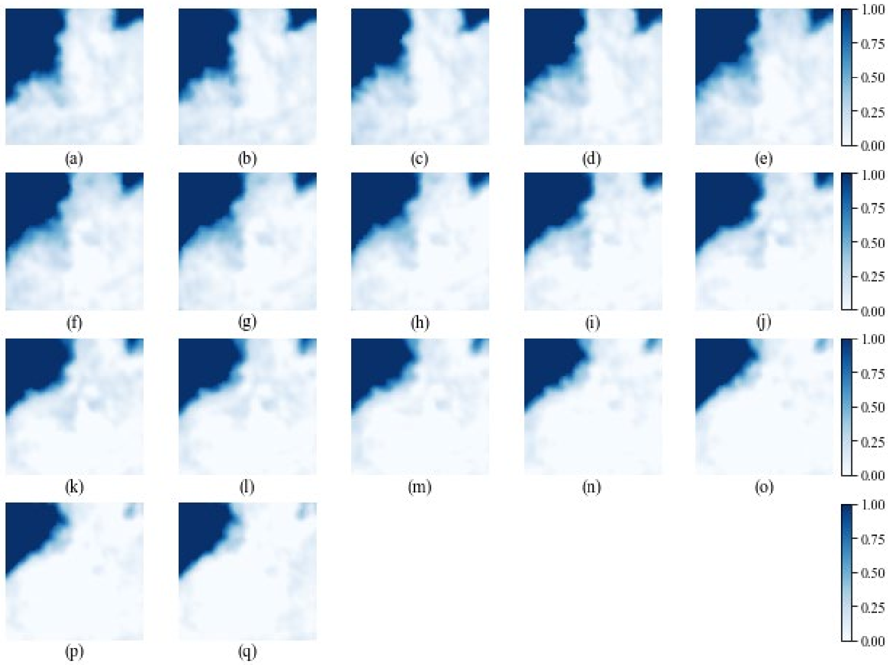

Figure 8: The actual daily evolution of sea ice in our focus area during a freezing cycle from (a) Oct 16th, 2022 to (q) Nov 1st, 2022.

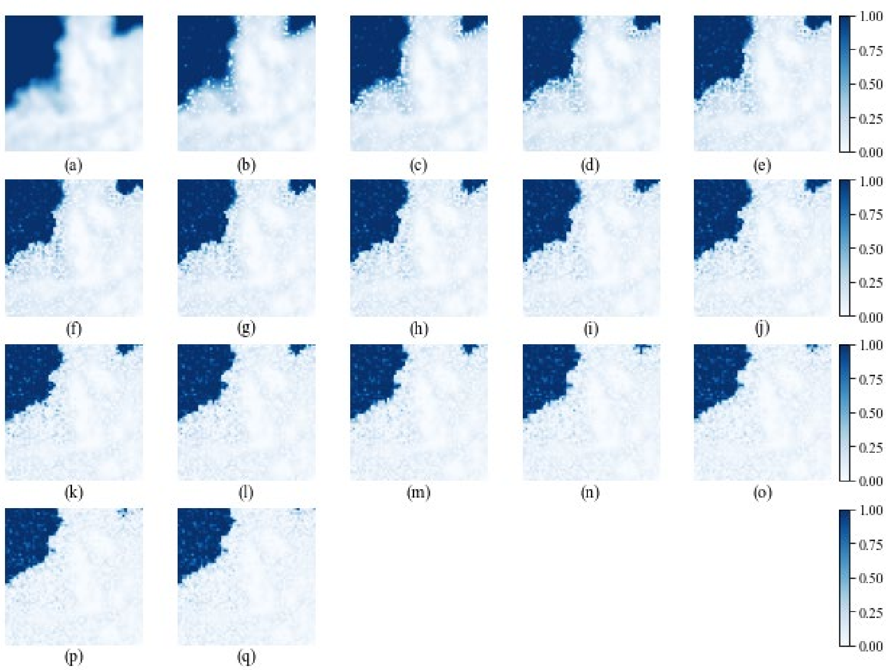

Figure 9: The simulated daily evolution of sea ice, based on the semi-monthly best-fit parameters, for our focus area during a freezing cycle from (a) Oct 16th, 2022 to (q) Nov 1st, 2022.

5.3 Simulation results for 2012

2012 recorded the lowest September Arctic sea ice extent in history [38]. Figure 10 shows the actual semi-monthly sea ice evolution in 2012 for our focus area. It can be observed that water covers approximately 75% of the area in peak September.

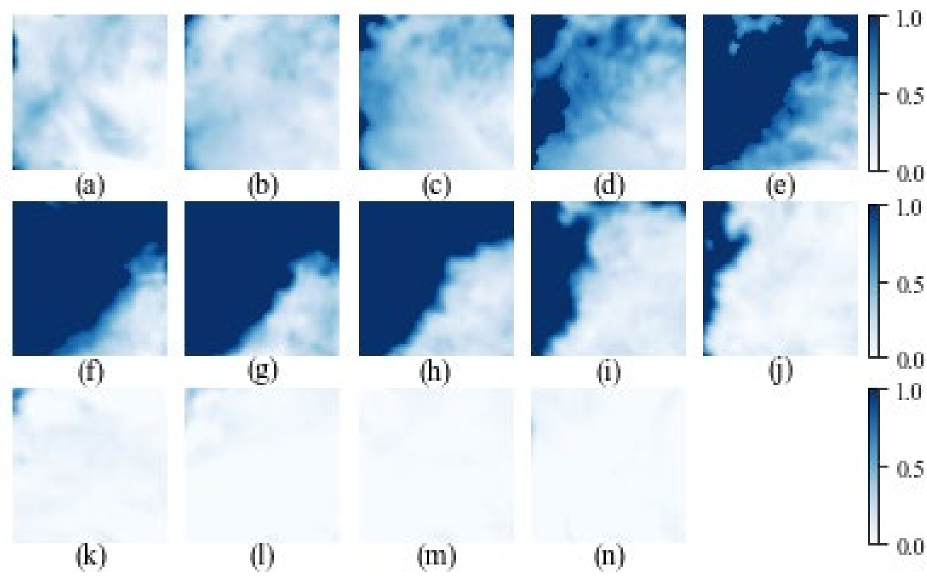

Figure 10: The actual semi-monthly evolution of sea ice in our focus area arctic sea in 2012: (a) June 16th, 2012, (b) July 1st, (c) July 16th, (d) Aug 1st, (e) Aug 16th, (f) Sept 1st, (g) Sept 16th, (h) Oct 1st, (i) Oct 16th, (j) Nov 1st, (k) Nov 16th, (l) Dec 1st, (m) Dec 16th, (n) Jan 1st, 2013.

Following the same steps as in Section 5.1, the IM simulation is conducted for 2012 for the focus area. The best-fit parameters are listed in Table 2 and the simulated images are shown in Figure 11. Comparison results for the average ice coverage percentage and the ice extent are shown in Figure 12. Like the 2022 results in Section 5.1, excellent match is observed between the IM simulation and the actual sea ice evolution. As can be seen, the simulated sea ice extent drops to the historic low level of 25% in Sept 2012 for our focus area.

	6/16 to 7/1	7/1 to 7/16	7/16 to 8/1	8/1 to 8/16	8/16 to 9/1	9/1 to 9/16	9/16 to 10/1	10/1 to 10/16	10/16 to 11/1	11/1 to 11/16	11/16 to 12/1	12/1 to 12/16	12/16 to 1/1/2013
J	4.5	4.6	4.6	4.7	5.3	4.5	5.4	4.7	4.7	5.0	5.3	5.3	5.4
Bo	4.4	5.6	6.3	7.5	7.0	0.3	-8.9	-14.0	-14.6	-14.8	-14.1	-15.0	-15.0
Bx	2.3	-7.7	-2.4	0.2	-9.5	-5.2	-7.2	-2.3	-3.4	-7.9	-8.6	-9.2	-9.6
By	6.5	-7.3	-5.5	-0.4	-9.7	3.0	-10.0	-9.3	-6.9	6.8	-5.5	5.1	0.4
I	11.0	11.0	11.0	10.5	10.2	10.9	9.3	9.3	9.1	10.1	10.5	10.9	10.9

Table 2: Best-fit parameters of 2012 sea ice evolution.

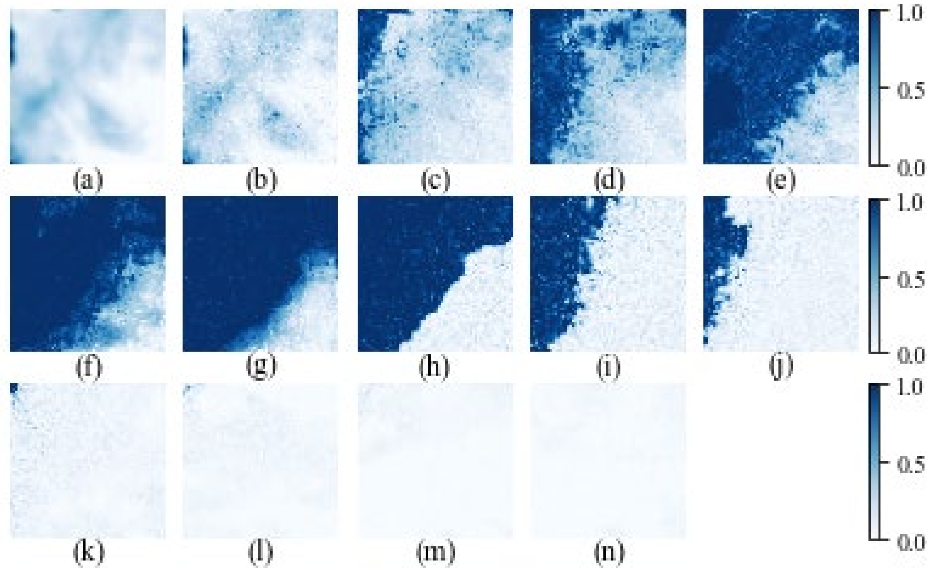

Figure 11**:** The simulated semi-monthly evolution of sea ice in our focus area arctic sea in 2012. (a) is the actual image on June 16th, 2012 as the start state; (b)-(n) are simulated images on (b) July 1st, (c) July 16th, (d) Aug 1st, (e) Aug 16th, (f) Sept 1st, (g) Sept 16th, (h) Oct 1st, (i) Oct 16th, (j) Nov 1st, (k) Nov 16th, (l) Dec 1st, (m) Dec 16th, and (n) Jan 1st, 2013.

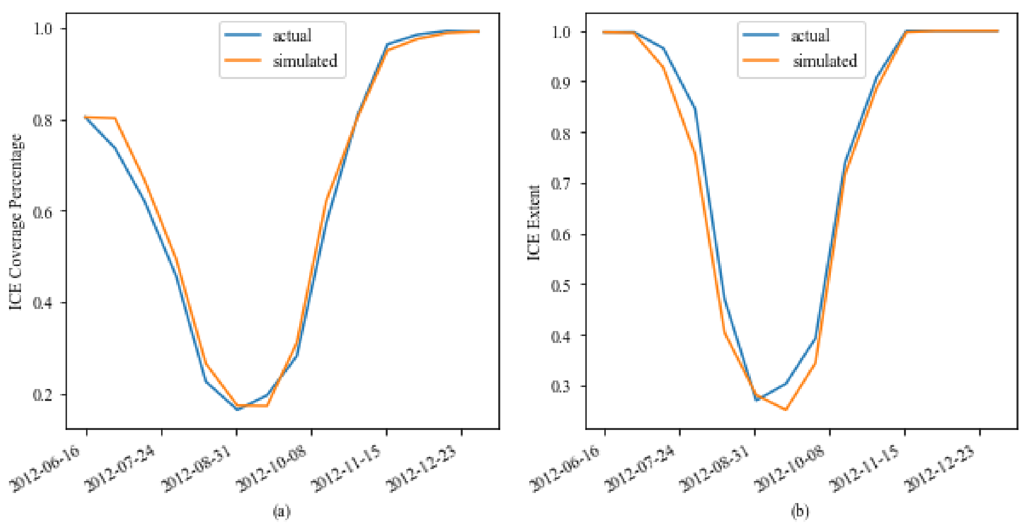

Figure 12: (a) The average ice coverage percentage in our focus area from June 16th, 2012 to Jan 1st, 2013; (b) The sea ice extent (the percentage of areas with at least 15% of ice coverage) from June 16th, 2012 to Jan 1st, 2013. Blue curves are the actual measures from the NRTSI data; orange ones show the IM simulation results.

5.4 Will 2023 break the 2012 record of Arctic sea ice extent?

The past month, July 2023, was reported as the hottest month on the earth on record. A natural question for us arises: will the Arctic sea ice extent break the 2012 minimum? The answer will reveal itself in about a month; in the meantime, let's see what our IM simulation predicts.

Following the same steps as in Section 5.1 and 5.3, the IM simulation is conducted for the period of June 16th to Aug 16th, 2023 in the focus area. Comparison of the actual and the simulated images are shown in Figure 13 and Figure 14, where reasonably good match is displayed. However substantial local irregularities are noticed especially in Figure 13 (d) and the IM simulation lacks the ability to capture them. It is not surprising to assume that these irregularities may be related to the extreme weather that the northern hemisphere just experienced in the past July.

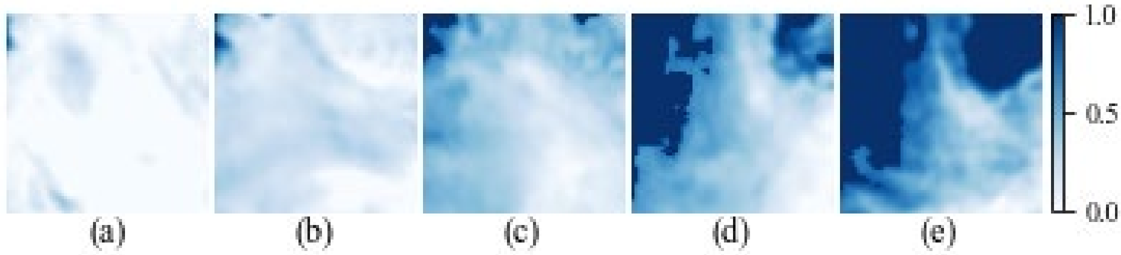

Figure 13: The actual semi-monthly evolution of sea ice in our focus area in 2023: (a) June 16th, 2023, (b) July 1st, (c) July 16th, (d) Aug 1st, (e) Aug 16th.

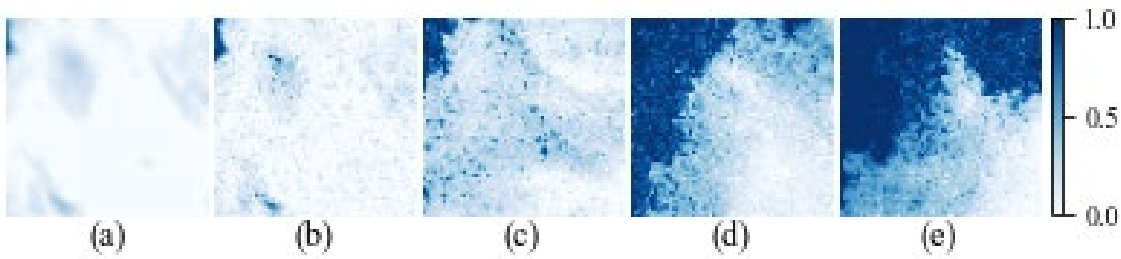

Figure 14: The simulated semi-monthly evolution of sea ice in our focus area in 2023: (a) is the actual image on June 16th, 2023 as the start state; (b)-(e) are simulated imaged on (b) July 1st, (c) July 16th, (d) Aug 1st, and (e) Aug 16th.

What will happen in the coming months of 2023? Based on the best-fit IM parameters from the corresponding periods in 2022, we can project how the sea ice will evolve in the future. In this process, we start with the actual configuration of the focus area as of Aug 16th, 2023, and run the simulation process for 9 periods forward till Jan 1st, 2024 with the IM parameters in Table 1. The projected images are shown in Figure 15, where the ice coverages in Sept 2023 (Figure 15 (b) & (c)) are predicted to be close to the 2012 levels in Figure 11 and Figure 12 , significantly lower than the corresponding periods in 2022 as in Figure 3 and Figure 4.

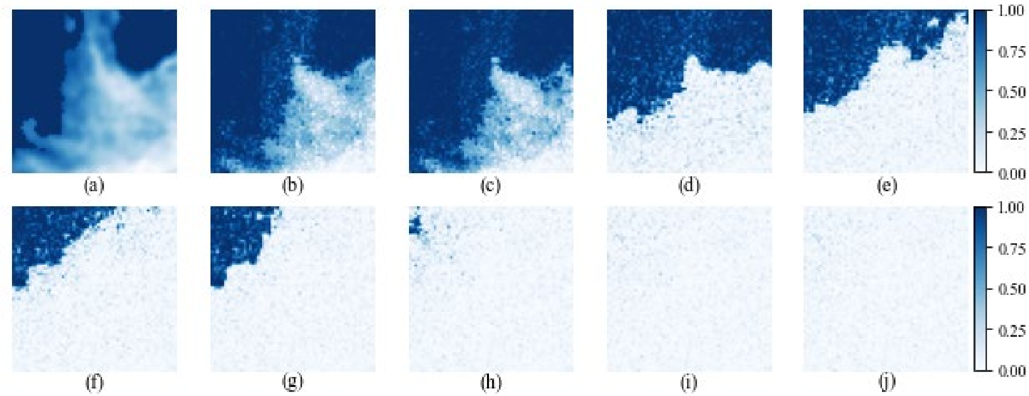

Figure 15: The simulated semi-monthly evolution of sea ice in our focus area in the near future. (a) is the actual image on Aug 16th, 2023 as the start state; (b)-(j) are simulated images (based on the best-fit IM parameters in the 2022 simulations over the corresponding semi-monthly periods) on (b) Sept 1st, (c) Sept 16th, (d) Oct 1st, (e) Oct 16th, (f) Nov 1st, (g) Nov 16th, (h) Dec 1st, (i) Dec 16th, and (j) Jan 1st, 2024.

For the 2023 projection, the two numerical measures, i.e., the average ice coverage percentage and the ice extent, are shown in Figure 16 against the available observations. The minimum of the sea ice extent in Figure 16 (b) is predicted to be 39%, marginally higher than the historical 2012 low level of 27% as shown in Figure 12 (b).

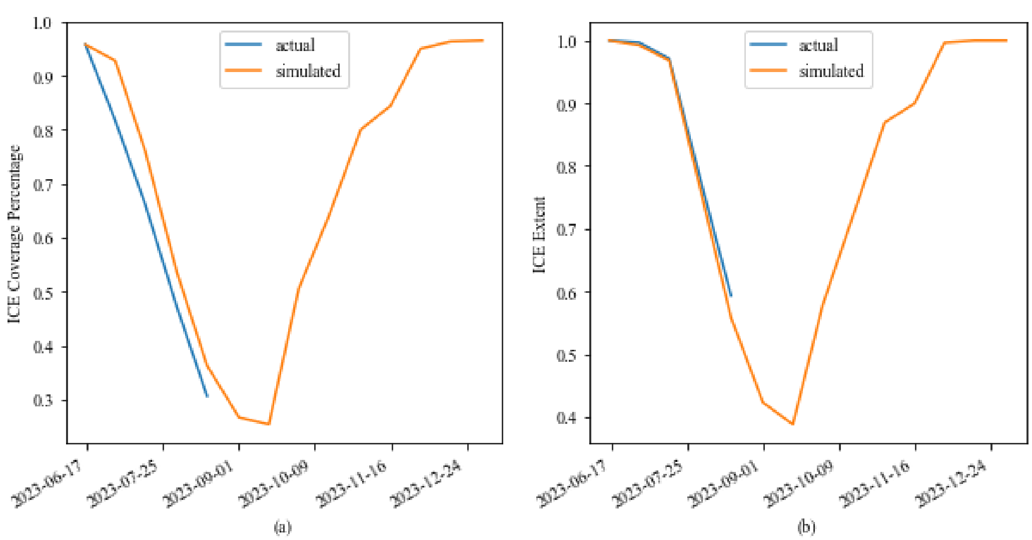

Figure 16: (a) The average ice coverage percentage in our focus area from June 16th, 2023 to Jan 1st, 2024; (b) The sea ice extent (the percentage of areas with at least 15% of ice coverage) from June 16th, 2023 to Jan 1st, 2024. Blue curves are the actual measures from the NRTSI data up to Aug 16th, 2023; orange ones show the IM simulation results.

The results in Figure 15 and Figure 16 are projections based on the IM parameters calibrated from the periods in 2022. These parameters, especially the external force factors B_0, B_x, B_y, vary with weather and environmental changes. Therefore, the accuracy of above projections in Figure 15 and Figure 16 will inevitably be limited. Nevertheless, they still provide us with reasonable guidance for the near future.

Even though our generalized IM offers an optimistic prediction that 2023 will not break the 2012 ice extent minimum, it projects that 2023 will set the second lowest in history, below the other previously achieved low levels in 2019 and 2020 [38]. (2019 and 2020 results are not included in this paper due to this paper length limitation, but these results will be provided upon request.) The NRTSI data to be released next month should soon tell us the truth.

6 Discussion and future work

In this paper, we introduce continuous spin values to a 2-D IM. The continuous Ising lattice is utilized to simulate the dynamics of the sea ice evolution in the Arctic region, with a generalized Metropolis-Hastings algorithm incorporating an inertia factor to overcome the resistance to the spin value change. The IM simulation results show excellent similarity with the actual sea ice dynamics, based on the ice configuration images and the numerical measures including the average ice coverage and the ice extent.

6.1 Will a "Blue Ocean Event" happen? If so, when will it be?

Based on our model and the simulation results, the Arctic sea ice extent in September 2023 is projected to be the second lowest in history, near the historic minimum set in 2012. As the Arctic sea ice continues to shrink, will the "Blue Ocean Event" happen, i.e., will we see an "ice-free" Arctic Ocean? Some research predicts that this can happen in the 2030s [39].

Our current model is unable to answer this "Blue Ocean Event" question thus far. As shown in Table 1 and Table 2, the best-fit IM parameters demonstrate substantial impact of external force factor B, which remains unexplored within the scope of our model. If the functional form of this external force is further enriched and linked to actual environmental factors in climate change modeling, the IM framework may prove powerful in providing the "Ising Model Prediction" to the "Blue Ocean Event" question.

6.2 Quantum Ising Model

This paper sets the stage for the future Ising model research on sea ice evolution. Methodologically, we generalize the classical Ising model with continuous spin values to incorporate varying ice/water percentages across the Ising lattice. An alternative idea to be explored in future research is the Quantum Ising Model (QIM), or the so-called Transverse Field Ising Model [40] [41]. With quantum computers, the continuous spin values can be naturally modeled by the rotation of qubits in the Bloch Sphere [42]. Large quantum computers are inaccessible for personal usage currently [43]; but once they are reachable, our research can be readily extended with the assistance of quantum computing in the future.

7 Supplemental materials

7.1 IM simulation results for other years

We also run the IM simulations for the Arctic sea ice evolution in our focus area in other years; these results can be provided upon request.

7.2 Computer codes and data

The computer programming for our research is done in Python. Computer codes and data can be shared upon request.

8 Bibliography

[1] E. Ising, "Beitrag zur Theorie des Ferromagnetismus," *Z. Phys,* vol. 31, no. 1, p. 2530258, 1925.

[2] E. Ising, Contribution to the Theory of Ferromagnetism, 1924.

[3] S. G. Brush, "History of the Lenz-Ising model," *Review of Modern Physics,* vol. 39, no. 4, p. 883, 1967.

[4] L. Onsager, "Crystal statistics. I. A two-dimensional model with an order-disorder transition," *Physical Review,* vol. 65, no. 3-4, pp. 117-149, 1944.

[5] M. Aguilera, S. A. Moosavi and H. Shimazaki, "A unifying framework for mean-field theories," *Nature Communications,* vol. 12, p. 1197, 2021.

[6] S. Sides, P. Rikvold and M. Novotony, "Kinetic Ising model in an oscilating field: finite-size scaling at the dynamic phase transition," *Physical review letters,* vol. 81, no. 4, p. 4865, 1998.

[7] D. Stauffer, "Social applications of two-dimensional Ising models," *American Journal of Physics,* vol. 76, no. 4, pp. 470-473, 2008.

[8] C. Campajola, F. Lillo and D. Tantari, "Inference of the kinetic Ising model with heterogeneous missing data," *Physical Review E,* vol. 99, no. 6, p. 062138, 2019.

[9] B. Dun and Y. Roudi, "Learning and inference in a nonequilibrium Ising model with hidden nodes," *Physical Review E,* vol. 87, no. 2, p. 022127, 2013.

[10] N. N. Vtyurina, D. Dulin, M. W. Docter, A. S. Meyer, N. H. Dekker and E. A. Abbondanzieri, "Hysteresis in DNA compaction by Dps is described by an Ising model," *Proceedings of the National Academy of Sciences,* vol. 113, no. 18, pp. 4982-4987, 2016.

[11] J. Majewski, H. Li and J. Ott, "The Ising model in physics and statistical genetics," *The American Journal of Human Genetics,* vol. 69, no. 4, pp. 853-862, 2001.

[12] A. Witoelar and Y. Roudi, "Neural network reconstruction using kinetic Ising," *BMC Neurosci.,* vol. 12, p. 274, 2011.

[13] C. Donner and M. Opper, "Inverse Ising problem in continuous time: a latent," *Physical Review E,* vol. 96, p. 061104, 2017.

[14] J. hertz, Y. Roudi and J. Tyrcha, "Ising model for inferring network structure from spike data," *In principles of Neural Coding,* pp. 527-546, 2013.

[15] Y. Roudi, D. B. and J. Hertz, "Multi-neuronal activity and functional connectivity in cell assemblies," *Curr. Opin. Neurobiol,* vol. 32, p. 38, 2015.

[16] Y. Shi and T. Duke, "Cooperative model of bacteril sensing," *Physical Review E,* vol. 58, no. 5, pp. 6399-6406, 1998.

[17] T. F. Stepinski, "Spatially explicit simulation of deforestation," *Environmental Research: Ecology.*

[18] T. F. Stepinskia and J. Nowosad, "The kinetic Ising model encapsulates essential dynamics of land pattern change," *bioRxiv,* 2023.

[19] Y.-P. Ma, I. Sudakov, C. Strong and K. Golden, "Ising model for melt ponds on Arctic sea ice," *New Journal of Physics,* vol. 21, p. 063029, 2019.

[20] T. C. Schelling, "Dynamic models of segregation," *J. Math. Sociol.,* vol. 1, pp. 143-186, 1971.

[21] J. P. Bouchaud, "Crises and collective socio-economic phenomena: simple," *J. Stat. Phys.,* vol. 151, p. 567, 2013.

[22] S. W. F. Bornholdt, "Stability of money: phase transitions," *Physica A: Statistical Mechanics and its Ap743,* vol. 316, no. 1-4, pp. 453-468, 2002.

[23] United States Environmental Protection Agency, "Climate Change Indicators: Arctic Sea Ice," 2021.

[24] R. Lindsey and M. Scott, "Climate Change: Arctic sea ice summer minimum," *Climate.gov,* 2022.

[25] N. L. R. C. A. S. D. Center, "Ice-Albedo Feedback in the Arctic," *NASA,* 2020.

[26] NSIDC, "Arctic sea ice news and analysis," 2021.

[27] NSIDC, "EASE-Grid sea ice age, version 4," 2021.

[28] World Meteorological Organization, "Copernicus confirms July 2023 was the hottest month ever recorded," 2023.

[29] L. Boltzmann, "Studies on the balance of living force between moving material points," *Wiener Berichte,* vol. 58, pp. 517-560, 1868.

[30] G. S. Sylvester and H. van Beijeren, "Phase Transitions for Continous-Spin Ising Ferromagnets," *Journal of Functional Analysis,* vol. 28, pp. 145-167, 1978.

[31] E. Bayong and H. T. Diep, "Effect of long-range interactions on the critical behavior of the continuous Ising model," *Physical Review B,* vol. 59, no. 18, p. 11919, 1999.

[32] M. Krasnytska, B. Berche, Y. YuHolovatch and R. Kenna, "Ising model with variable spin/agent strengths," *Journal of Physics: Complexity,* vol. 1, p. 035008, 2020.

[33] W. N. J. S. S. H. W. M. A. H. a. D. J. S. Meier, "Near-Real-Time DMSP SSMIS Daily Polar Gridded Sea Ice Concentrations, Version 2," NASA National Snow and Ice Data Center Distributed Active Archive Center, Boulder, Colorado USA, 2023.

[34] G. J. Roy, "Roy J. Glauber "Time-Dependent Statistics of the Ising Model," *Journal of Mathematical Physics,* vol. 4, no. 2, pp. 294-307, 1963.

[35] N. Metropolis, A. W. Rosenbluth, M. N. Rosenbluth, A. H. Teller and E. Teller, "Equation of State Calculations by Fast Computing Machines," *J. Chem Phys,* vol. 21, no. 6, p. 1087, 1953.

[36] C. Tsallis and D. Stariolo, "Generalized Simulated Annealing," *Physica A,* vol. 233, pp. 395-406, 1996.

[37] Y. Xiang, D. Sun, W. Fan and X. Gong, "Generalized Simulated Annealing Algorithm and Its Application to the Thomson Model," *Physics Letters A,* vol. 233, pp. 216-220, 1997.

[38] NASA , "Arctic Sea Ice Minimum Extent," 2022.

[39] Y.-H. Kim, S.-K. Min, N. P. Gillett, D. Notz and E. Malinina, "Observationally-constrained projections of," *Nature Communications,* vol. 14, p. 3139, 2023.

[40] P. Pferty, "The one-dimensional Ising model with a transverse field," *Annals of Physics,* pp. 79-90, 1970.

[41] B. K. Chakrabarti, A. Dutta and P. Sen, Quantum Ising Phases and Transitions in Transverse Ising Models, Berlin: Springer, 1996.

[42] M. A. Nielsen and I. L. Chuang, Quantum Computation and Quantum Information, Cambridge University Press, 2004.

[43] M. I. Dyakonov, Will We Ever Have a Quantum Computer?, Springer, 2020.